World Academy of Science, Engineering and Technology
International Journal of Mechanical and Mechatronics Engineering
Vol:8, No:11, 2014

Three-Dimensional Numerical Simulation of Drops Suspended in Poiseuille Flow: Effect of Reynolds Number

A. Nourbakhsh

***Abstract*—**A finite difference/front tracking method is used to study the motion of three-dimensional deformable drops suspended in plane Poiseuille flow at non-zero Reynolds numbers. A parallel version of the code was used to study the behavior of suspension on a reasonable grid resolution (grids). The viscosity and density of drops are assumed to be equal to that of the suspending medium. The effect of the Reynolds number is studied in detail. It is found that drops with small deformation behave like rigid particles and migrate to an equilibrium position about half way between the wall and the centerline (the Segre-Silberberg effect). However, for highly deformable drops there is a tendency for drops to migrate to the middle of the channel, and the maximum concentration occurs at the centerline. The effective viscosity of suspension and the fluctuation energy of the flow across the channel increases with the Reynolds number of the flow.

***Keywords*—**Suspensions, Poiseuille flow, Effective viscosity, Reynolds number.

I. Introduction

THE flow of suspensions of deformable particles, such as drops, cells and capsules has been a matter of interest for many years. The flow of slurries, microfluidic systems, oil recovery by chemical flooding, advanced materials processing, waste treatments and food processing is typical application of these flows. In these applications, it is often necessary to predict or manipulate the rheology of suspensions. The rheological properties of suspensions depend on a number of parameters including the volume fraction, initial spatial distribution, particle size distribution, the structural constitution and associated mechanical properties of the interfaces. The dynamic interaction of these factors determines the suspension microstructure, from which the macroscopic rheological properties develop. Predicting the rheological behavior of suspensions has been a long-standing challenge in continuum and statistical mechanics.

The migration of dilute suspensions of neutrally buoyant solid particles in pipe flow was first observed by Segre and Silberberg [2], [3] at finite Reynolds numbers. They found that the particles migrate away from both the wall and the centerline and accumulate at a certain equilibrium position about 0.6 times the tube radius. The remarkable Segre-Silberberg effect has been verified by many experimental works. For example, Golsmith & Mason [4] observed that a rigid particle stayed at its initial radial position at very small Reynolds numbers and migrated to intermediate positions at finite Reynolds numbers. While experiments of Goldsmith and Mason used mostly a single drop and dilute suspensions, Kowalewski [1] conducted experiments on concentrated suspension of drops and measured the concentration and velocity profiles of droplet suspensions flowing through a tube. An experimental study of the migration of dilute suspensions of particles in Poiseuille flow in a wide range of Reynolds numbers (67-1700) was performed by Matas et al. [5] They extended the results of Segre and Silberberg and showed that the tubular pinch effect in which particles accumulate is moved toward the wall as the Reynolds number increases.

Several authors have simulated detailed motion of random and ordered suspensions numerically. Zhou & Pozrikidis [6] simulated the pressure-driven flow of a periodic suspension of drops by a boundary integral method and showed that when the viscosity of drops is the same as that of the suspending fluid, the drops migrate towards the centerline of the channel. A single drop with a viscosity ratio of 10 moves to an equilibrium position at about halfway between the wall and the centerline. Nott & Brady [7] simulated the pressure-driven flow of a non-Brownian suspension at zero Reynolds number using Stokesian Dynamics. They indicated that the particles gradually migrate towards the centre of the channel, resulting an in homogeneous concentration profile and a blunting of the velocity profile. Simulations of a concentrated suspension of several three-dimensional drops in a linear shear flow have been conducted by Loewenberg & Hinch [8]. They observed a shear thinning behavior for the suspension, and in contrast to rigid particles, the viscosity of the emulsion weakly increased with volume fraction. Three-dimensional numerical simulations on the motion of a large number of deformable cells in micro channels were presented by Doddi & Bagchi [9] by an immersed boundary method. They analyzed the three dimensional trajectories and velocity fluctuations of individual cells in the suspension. Results of dynamic simulations of the pressure-driven flow of a two-dimensional suspension in a channel confined between two parallel walls were considered by Li & Pozrikidis [10]. They illustrated the effect of the Capillary number and viscosity ratio on the distribution of drops across the channel width and the effective viscosity of suspension.

Feng, Ho & Joseph [11], [12] conducted a two-dimensional finite element simulation of the motion of a solid particle in a

A. Nourbakhsh is with the Department of Mechanical Engineering, Bu-Ali Sina University, Hamedan, Iran (e-mail: nourbakhsh@ basu.ac.ir).

Couette and a Poiseuille flow at finite Reynolds numbers. They observed that a neutrally buoyant particle exhibits the Segre-Silberberg effect in Poiseuille flow. Mortazavi & Tryggvasson [13] used a finite-difference / front tracking method to study the motion of two- and three-dimensional drops suspended in pressure-driven channel flow at finite Reynolds numbers. They observed that in the limit of a small Reynolds number, the motion of the drop depends strongly on the viscosity ratio. At a higher Reynolds number, the drop moves to an equilibrium position about halfway between the centerline and the wall or it undergoes oscillatory motion. The motion of a neutrally buoyant three-dimensional drop between two parallel plates has been simulated by Nourbakhsh & Mortazavi [14]. They found that a neutrally buoyant drop migrates to an equilibrium lateral position about halfway between the wall and the centerline at finite Reynolds numbers. Bayareh and Mortazavi [15] presented results of simulation of cross-stream migration of a drop in simple shear flow at finite Reynolds numbers. They showed that a drop migrates to the centerline of the channel in a shear flow. The motion of two-dimensional deformable drops suspended in a linear shear flow at non-zero Reynolds numbers was studied by Mortazavi et al [16]. They studied the lateral migration of a drop and observed that at a relatively high Reynolds number and small deformation, the drop migrates to an equilibrium position, which is a little off the channel centerline. They also simulated the suspension of 36 drops and found that suspension of drops at finite Reynolds numbers exhibits a shear thinning behavior. Bayareh and Mortazavi [17] simulated the collision of two equal-size drops in an immiscible phase undergoing a shear flow. The size and vertical distribution of drops in dispersed liquid-liquid pipeline flows were studied experimentally by Lovick & Angeli [18]. They measured drop velocities at different locations in a pipe cross section and observed that the mixture velocity did not affect the drop size of either phase significantly.

Here, we present simulations of suspensions of three-dimensional deformable drops in a periodic channel at finite Reynolds numbers. The simulations yield information on the effects of the Reynolds number. 27 drops are suspended in a 3 by 3 by 3 arrangements inside the channel. Drops are initially organized as a regular array and their relative positions are slightly perturbed. The relative size of drops are $\zeta = 0.121$ and $\zeta = 0.138$ for volume fractions; $\phi = 0.2$ and $\phi = 0.3$ respectively.

II. Governing Equations and Numerical Method

A. Problem Setup

The geometry of the flow is shown in Fig. 1. The motion of drops is studied in a channel that is bounded by two flat plates in the z direction. The height, depth and length of the channel are the same. In absence of drops, the flow is a fully-developed parabolic flow and is driven by a constant pressure gradient. We decompose the pressure gradient in the channel as [13]:

$$\nabla p = \nabla p_o + \nabla p' \tag{1}$$

where ∇p_o is the external specified pressure gradient and $\nabla p'$ is the perturbation pressure gradient to be computed as part of the solution. Gravity is neglected and buoyancy effects are absent.

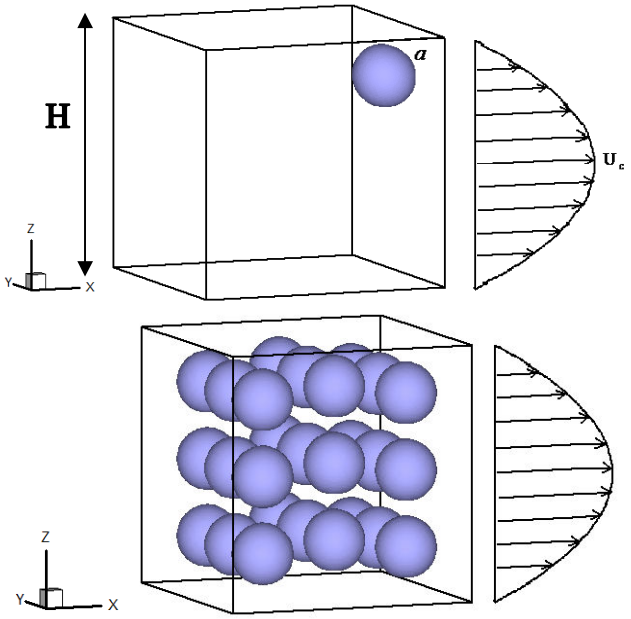

Fig. 1 The geometry for the simulation of drops in a channel

B. Governing Equations

The governing equations for the flow of multi-fluid systems are the Navier-Stokes equations. In conservative form they are:

$$\frac{\partial \rho \mathbf{u}}{\partial t} + \nabla.(\rho \mathbf{u}\mathbf{u}) = -\nabla p + \rho \mathbf{f} + \nabla.\mu(\nabla \mathbf{u} + \nabla^{T}\mathbf{u}) + \int \sigma \kappa' \mathbf{n}' \delta^{\beta}(\mathbf{x} - \mathbf{x}')ds' \tag{2}$$

where, $\mathbf{u}$ is the velocity, p is the pressure, ρ and μ are the discontinuous density and viscosity fields respectively. σ is the surface tension coefficient, $\mathbf{f}$ is a body force and the surface tension force is added at the interface. The term δ^{β} is a two- or three-dimensional δ function constructed by repeated multiplication of one-dimensional δ functions. κ is the curvature for two-dimensional flow and twice the mean curvature for three-dimensional flows. $\mathbf{n}$ is a unit vector normal to the front, $\mathbf{x}$ is the position in Eulerian coordinate, and $\mathbf{x}'$ is a Lagrangian representation of the interface.

The Navier-Stokes equations are solved by a second-order projection method using centred differences on a fixed staggered grid. Both the drop and the ambient fluid are taken to be incompressible, so the velocity field is divergence free:

$$\nabla.\mathbf{u} = 0 \tag{3}$$

Equation (3), when combined with the momentum equation, leads to a non-separable elliptic equation for the pressure. If the density is constant, the elliptic pressure equation is solved by fast Poisson solver (FISHPACK), but when the density of the drop is different from the suspending fluid, the equation is solved by a multigrid method [19].

Equations of state for the density and the viscosity are:

$$\frac{D\mu}{Dt} = 0 \text{ , } \frac{D\rho}{Dt} = 0 \tag{4}$$

Equation (4) states that the density and the viscosity of a fluid particle remain constant.

C. Boundary Conditions

The boundary condition on the plates is the no-slip condition. The domain is periodic in the x- and y-directions. Normal stress shows a jump across the interface by surface tension and tangential stresses are continuous across the surface of drop.

D. Dimensionless Parameters

The governing non-dimensional numbers are as follows: the ratio of the viscosity of the drop fluid to the suspending medium $\lambda = \mu_i / \mu_o$, the density ratio $\alpha = \rho_i / \rho_o$ (the viscosity and density of the drop liquid are denoted by μ_i and ρ_i, respectively, and the suspending fluid has viscosity μ_o and density ρ_o), the ratio of the radius of the drop to channel height $\zeta = a / H$, the volume fraction ϕ, the bulk Reynolds number is defined in terms of the undisturbed channel centerline velocity (U_c), and the channel height, $\mathrm{Re}_b = \rho_o U_c H / \mu_o$, the particle Reynolds number is defined as $\mathrm{Re}_p = \rho U_c a^2 / \mu H$, the Capillary number describes the ratio of the viscous stress to the interfacial tension, $\mathrm{Ca} = \mathrm{U_c} \mu_o / \sigma$.

The effective viscosity of suspension is defined as $\mu_{eff} = \mu_o Q_p / Q$, where Q_p is the volume flow rate through the channel without drops ($Q_p = 2U_c H / 3$), and Q is the actual flow rate through the channel subject to the same pressure gradient.

E. Numerical Method

Different numerical methods are developed for simulating flows with interfaces. These methods can be divided into two groups, depending on the type of grids used: moving grid and fixed grid. Two important approaches of fixed-grid methods are the volume-of-fluid (VOF) and level-set method. The volume-of-fluid method uses a marker function. The main difficulty in using VOF method is the maintenance of a sharp boundary between two phases and the computation of the surface tension. The level-set method defines the interface by a level-set function, but this approach has some difficulties in preserving the mass conservation. There are recent efforts in conserving mass in level-set method (see for example [20]. Here, a finite difference/front tracking method is used. This approach was described in detail by Unverdi & Tryggvason [21], [22], Tryggvason et al. [23] and only a brief outline is given here. The Navier-Stokes equations are solved by a second-order projection method using centred differences on a fixed, staggered grid. To keep the boundary between the drop and the ambient fluid sharp, and to accurately compute the surface tension, the boundary is represented by connected marker points (the front) that are advected by the flow velocity, interpolated from the fixed grid. To maintain the front resolution, new marker points are inserted when the distance between points becomes too large. Points are also deleted if the distance between two points becomes smaller than a prescribed value. The singularities at the front (density and viscosity gradients and surface tension) are approximated on the fixed grid by smooth functions with a compact support. The density and viscosity fields are reconstructed at each time step by integrating the smooth grid delta function, after the front has been moved, and the body force due to surface tension is added to the nodal values of the discrete Navier-Stokes equations. As drops move and deform, the density and the viscosity need to be updated. This is done by solving a Poisson equation for an indicator function $I(x)$ such that:

$$\rho(\mathbf{x}) = \rho_\mathrm{o} + (\rho_\mathrm{i} - \rho_\mathrm{o}) I(\mathbf{x}) \tag{5}$$

$$\mu(\mathbf{x}) = \mu_\mathrm{o} + (\mu_\mathrm{i} - \mu_\mathrm{o}) I(\mathbf{x}) \tag{6}$$

A new version of the code written for parallel machines was used in the current study. The parallelization method combines a domain decomposition approach for the field or Eulerian quantities and a master-slave approach for the front, where each front has a master processor that gathers data from the other (slave) processors which share this front. Unlike the serial code, there is not one single linked list for all the fronts; rather, each front is represented by its own linked list.

III. Results

A. Resolution Test and Validation:

We investigate the depending of the results to grid resolution by considering three grid resolutions ($64\times64\times64$, $128\times128\times128$ and $256\times256\times256$ grid points). 27 drops with a relative size of $\zeta = 0.121$ are initially released inside the channel. Drops are placed in a regular array (3 by 3 by 3) and their relative positions are slightly perturbed. The flow parameters are: $\mathrm{Re_b} = 20$, $Ca = 0.05$, $\alpha = \lambda = 1$ and $\phi = 0.2$. Fig. 2 shows the relative viscosity of suspension versus time at three grid resolutions. There is a slight change in the relative viscosity when the grid is refined from the coarse grid to intermediate one. However, the difference between the relative viscosity for the two fine grids is almost negligible. This is an indication of the convergence of the results as the grid is refined.

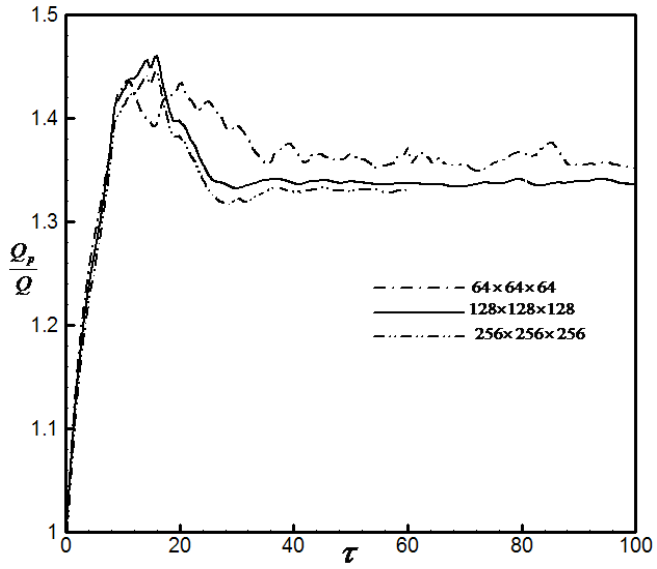

Fig. 2 The relative viscosity versus non-dimensional time at three different grid resolutions

To validate the results of the current study, a case with low Reynolds number is considered, and it is compared with that considered by Doddi & Bagchi [9] for zero Reynolds number. The steady state velocity profile is plotted in Fig. 3. Other flow conditions ($\mathrm{Re}_b = 20$) as well as the Newtonian velocity profile are also plotted for comparison.

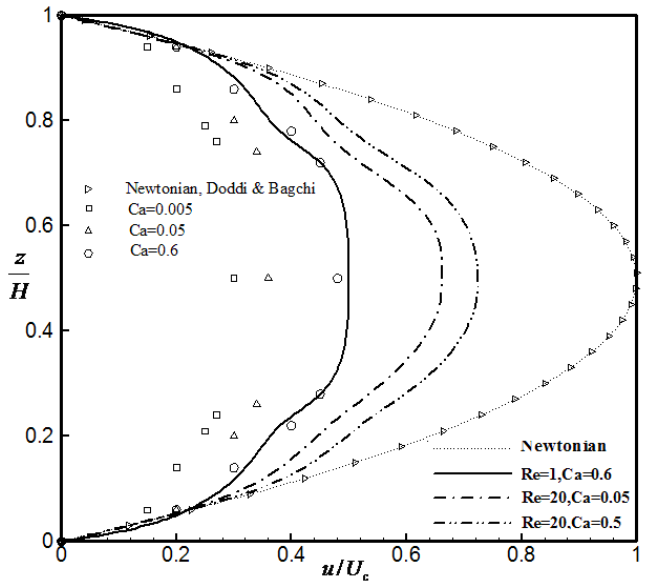

Fig. 3 Average velocity profiles and the corresponding Newtonian velocity profile

The steady state velocity profile obtained in the present study for $\mathrm{Re}_b = 1$ and $Ca = 0.6$ is close to that found by Doddi & Bagchi [9] at zero Reynolds number.

B. Effect of the Reynolds Number

We present results that show the effect of the Reynolds number on the concentration of drops across the channel and the effective viscosity of suspension. Two Capillary numbers are examined ($Ca = 0.05$, 0.8). Fig. 4 shows the concentration of drops across the channel for three Reynolds numbers ($\mathrm{Re}_b = 10$, 20 and 40). For almost rigid drops ($Ca = 0.05$), two peaks are observed close the channel walls.

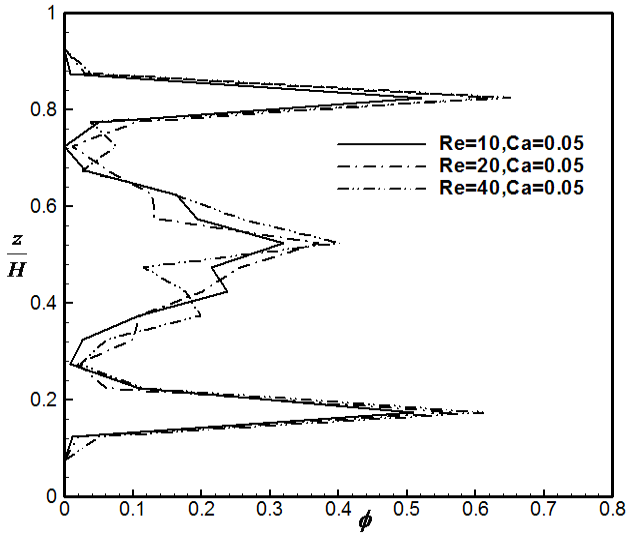

(a)

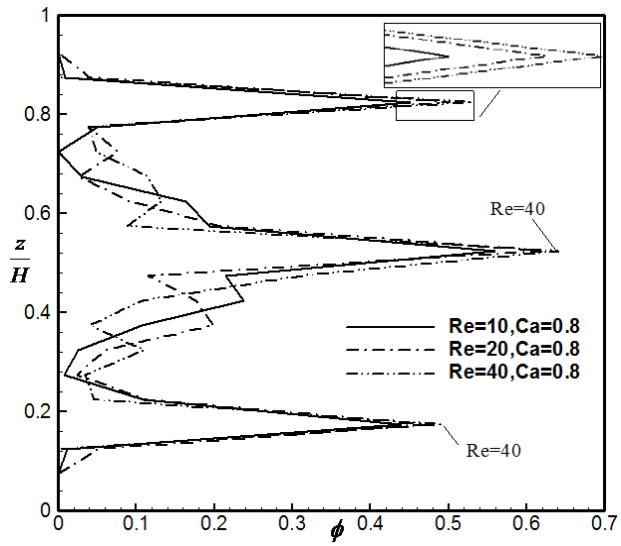

(b)

Fig. 4 The density distribution of drops across the channel for the simulation of 27 drops with three different Reynolds numbers

The flow is dominated by inertia and deformation plays no significant role. The peaks get larger as the Reynolds number is raised. For highly deformable drops ($Ca = 0.8$) the maximum peak is at the centerline. Also the peaks increase in magnitude as the Reynolds number increases (Fig. 4 (b)) which is an inertia effect.

The relative viscosity of suspension is plotted in Fig. 5 for different Reynolds numbers and Capillary numbers. The effective viscosity increases with the Reynolds number. This

is mainly due to interaction between drops that is pronounced as the Reynolds number increases. The figure also shows a case with low Reynolds number ($\mathrm{Re}_b = 1$) which is an indication of small inertia limit.

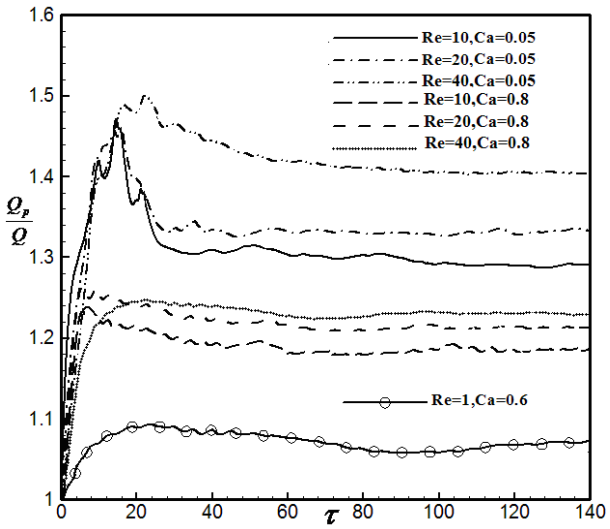

Fig. 5 The relative viscosity versus non-dimensional time at different Reynolds numbers

The fluctuation energy of the flow is plotted across the channel width for different Reynolds numbers in Fig. 6. The fluctuation energy was computed from:

$$< u'u'(z) >= (\sum_{j=1}^{N}\sum_{i=1}^{M}[u_{i,j}(z) - u_{avg}(z)]^2 + \sum_{j=1}^{N}\sum_{i=1}^{M} v_{i,j}^2(z) + \sum_{j=1}^{N}\sum_{i=1}^{M} w_{i,j}^2(z))/(M \times N) \quad (7)$$

Here $u_{i,j}$ is axial velocity, $v_{i,j}$ and $w_{i,j}$ are the velocity components in the y- and z-directions respectively, and $u_{avg}(z)$ is the average axial velocity at a distance z from the lower wall. *M* and *N* are the number of grid points in x- and y-directions respectively. This fluctuation energy is averaged over time after an initial transition period. Following Nott & Brady [7], the fluctuation energies are scaled using the square of the average shear velocity (au_{avg}/H). The fluctuation energy is larger in the wall regions where the shear rate is large. It gets minimum at the center of channel where the shear rate is almost zero, and the interaction between drops is weak. As expected the fluctuation energy increases as the Reynolds number is raised. Since the flow is simulated at finite Reynolds numbers, the inertia of the flow is included in the simulations. As a result, we observe an increase in the fluctuation energy (suspension temperature) with the Reynolds number.

We also present the Reynolds stresses developed in the flow of suspension. The Reynolds stresses are plotted as a function of time in Fig. 7. The Reynolds stresses are scaled by the square of the average shear velocity (au_{avg}/H). The Reynolds stresses is plotted for different Reynolds numbers. Results show that the Reynolds stress has reached a nearly stationary state. The normal component of the Reynolds stresses (*Rxx)* obtains positive mean values. It also enhances as the Reynolds number increases.

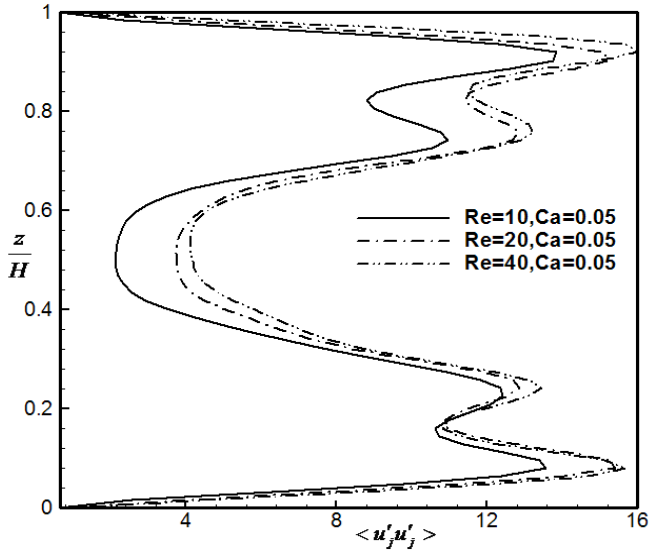

Fig. 6 The variation of the fluctuation energy across the channel width for simulations with different Reynolds numbers

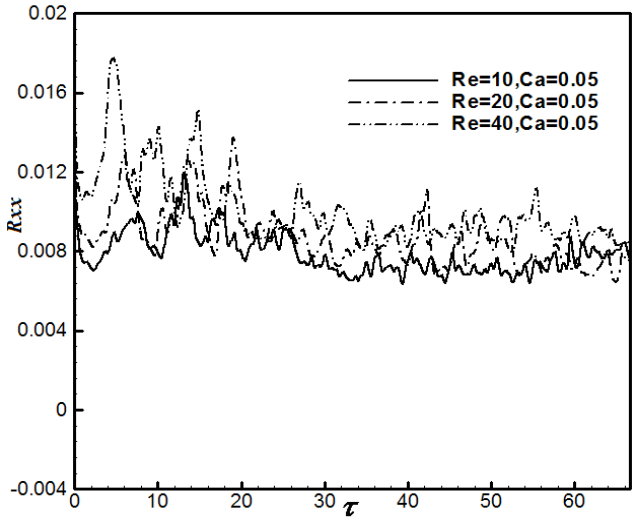

Fig. 7 The Reynolds stress as a function of non-dimensional time for different Reynolds numbers

IV. Conclusion

In the present study, a finite difference / front tracking method has been used for simulation of the motion of several three-dimensional drops suspended in plane Poiseuille flow, accounting for the effect of inertia. Very few works exist that attempt to consider interaction of multiple drops in a dense suspension.

The simulations for a system of 27 drops in a periodic channel showed that nearly spherical drops gradually migrate to a location between the channel axis and the walls (the Segre-Silberberg effect), resulting in a considerably inhomogeneous distribution and a blunting velocity profile at

steady state. The presence of drops causes a blunting of velocity profile across the channel. The fluctuation energy of the flow across the channel (suspension temperature) was also computed for different flow conditions. It is of interest because it is closely related to the diffusivity of suspension. The fluctuation energy is lowest in the middle of channel where the shear rate is small and the interaction between drops is weak. It increases as one moves away from the channel centerline and becomes maximum close to the walls. It vanishes in the wall regions where no drops are present.

The effect of the Reynolds number was investigated by considering four Reynolds numbers (1, 10, 20, 40) and two Capillary numbers (0.05,0.8). At a low Capillary number (0.05), the flow is dominated by inertia and the peaks in the density distribution of drops in the wall regions enhance as the Reynolds number is raised. Also for a large Capillary number (0.8), the large peak at the middle of channel enhances with Reynolds number. The fluctuation energy of the flow across the channel increases as the Reynolds number increases. The variation of the Reynolds stress with the Reynolds number was also investigated. The normal component (*Rxx)* obtains positive values and it increases as the Reynolds number is raised.

REFERENCES

[1] G. Segre, and A. Silberberg, "Behaviour of macroscopic rigid spheres in poiseuille flow, part1. determination of local concentration by statistical analysis of particle passages through crossed light beams," *J. Fluid Mech*. vol. 14, 1962a, pp. 115.

[2] G. Segre, and A. Silberberg, "Behaviour of macroscopic rigid spheres in poiseuille flow, part2. experimental results and interpretation," *J. Fluid Mech*. vol. 14, 1962b, pp. 136.

[3] H. L. Goldsmith, and S. G. Mason, "The flow of suspensions through tubes. I. Single spheres, rods and discs," *J. Colloid Sci.* vol. 17, 1962, pp. 448.

[4] T. A. Kowalewski, "Concentration and velocity measurement in the flow of droplet suspensions through a tube," *Experiments in Fluids.* vol. 2, 1984, pp. 213.

[5] J. P. Matas, J. F. Morris, and E. Guazzelli, "Inertial migration of rigid spherical particles in Poiseuille flow," *J. Fluid Mech.* vol. 515, 2004, pp. 171.

[6] H. Zhou, and C. Pozrikidis, "Pressure-driven flow of suspensions of liquid drops," *Phys. Fluids*. vol. 6, 1994, pp. 80.

[7] P. Nott, and J. Brady, "Pressure-driven flow of suspensions: simulation and theory," *J. Fluid Mech*. vol. 275, 1994, pp. 157.

[8] M. Loewenberg, and E. J. Hinch, "Numerical simulation of a concentrated emulsion in shear flow," *J. Fluid Mech*. vol. 321, 1996, pp. 395.

[9] S. K. Doddi, and P. Bagchi, "Three-dimensional computational modeling of multiple deformable cells flowing in micro vessels," *Physical Review E.* vol. 79, 2009, pp. 046318-1.

[10] X. Li, and C. Pozrikidis, "Wall-bounded shear flow and channel flow of suspensions of liquid drops," *Int. J. Multiphase Flow*. vol. 26, 2000, pp. 1247.

[11] D. J. Feng, H. H. Hu, and D. D. Joseph, "Direct simulation of initial value problems for the motion of solid bodies in a Newtonian fluid. Part1. Sedimentation," *J. Fluid Mech*. vol. 261, 1994a, pp. 95.

[12] D. J. Feng, H. H. Hu, and D. D. Joseph, "Direct simulation of initial value problems for the motion of solid bodies in a Newtonian fluid. Part2. Couette and Poiseuille flows," *J. Fluid Mech*. vol. 277, 1994b, pp. 271.

[13] S. S. Mortazavi, and G. Tryggvason, "A numerical study of the motion of drops in poiseuille flow, part1: Lateral migration of one drop," *J. Fluid Mech.* vol. 411, 2000, pp. 325.

[14] A. Nourbakhsh, S. S. Mortazavi, "A three-dimensional study of the motion of a drop in plane Poiseuille flow at finite Reynolds numbers," *Iranian J. Science and Technology, Transaction B: Engineering*. vol. 34, No. B2, 2010, pp. 179.

[15] M. Bayareh, and S. S. Mortazavi, "Numerical simulation of the motion of a single drop in a shear flow at finite Reynolds numbers," *Iranian J. Science and Technology, Transaction B: Engineering.* vol. 33, No. B5, 2009, pp. 441.

[16] S. S. Mortazavi, Y. Afshar, and H. Abbuspour, "Numerical simulation of two-dimensional drops suspended in simple shear flow at nonzero Reynolds numbers," *J. Fluids. Eng*. vol. 133, 2011, pp. 031303-1.

[17] M. Bayareh, and S. S. Mortazavi, "Binary collision of drops in simple shear flow at finite Reynolds numbers: Geometry and viscosity ratio effects," *Advances in Eng. Software*. vol. 42, 2011, pp. 604.

[18] J. Lovick, and P. Angeli, "Droplet size and velocity profiles in liquid-liquid horizontal flows," *Chem. Eng. Sci.* vol. 59, 2004, pp. 3105.

[19] J. Adams, "MUDPACK: Multigrid FORTRAN software for the efficient solution of linear elliptic partial differential equations," *Appl. Math. Comput.* vol. 34, 1989, pp. 113.

[20] M. Gorokhovski, and M. Herrmann, "Modeling primary atomization," *Annual Review of Fluid Mech*. vol. 40, 2008, pp. 343.

[21] S. O. Unverdi, and G. Tryggvason, "A front-tracking method for viscous incompressible multi-fluid flows," *J. Comput. Phys*. vol. 100, 1962a, pp. 25.

[22] S. O. Unverdi, and G. Tryggvason, "Computations of multi-fluid flows." *Physics*. vol. 60(D), 1962b, pp. 70.

[23] G. Tryggvason, B. Bunner, A. Esmaeeli, D. Juric, N. Al-Rawahi, W. Tauber, J. Han, S. Nas, and Y. J. Jan, "A front-tracking method for the Computations of Multiphase Flow," *J. Computational Physics*. vol. 169, 2001, pp. 708.